Robotica (2018) volume 36, pp. 1386–1401. © Cambridge University Press 2018
doi:10.1017/S0263574718000073

Kinematic accuracy research of 2(3HUS+S) parallel manipulator for simulation of hip joint motion

Huizhen Zhang, Gang Cheng*, Xianlei Shan and Feng Guo

School of Mechatronic Engineering, China University of Mining and Technology, 221116 Xuzhou, P. R. China

(Accepted January 8, 2018. First published online: June 6, 2018)

SUMMARY

In this paper, the kinematic accuracy problem caused by geometric errors of a 2(3HUS+S) parallel manipulator is described. The kinematic equation of the manipulator is obtained by establishing a D–H (Denavit–Hartenberg) coordinate system. A D–H transformation matrix is used as the error-modeling tool, and the kinematic error model of the manipulator integrating manufacturing and assembly errors is established based on the perturbation theory. The iterative Levenberg–Marquardt algorithm is used to identify the geometric errors in the error model. According to the experimentally measured attitudes, the kinematic calibration process is simulated using MATLAB software. The simulation and experiment results show that the attitude errors of the moving platforms after calibration are reduced compared with before the calibration, and the kinematic accuracy of the manipulator is significantly improved. The correctness and effectiveness of the error model and the kinematic calibration method of the 2(3HUS+S) parallel manipulator for simulation of hip joint motion are verified.

KEYWORDS: 2(3HUS+S) parallel manipulator, Kinematic accuracy, Error model, Kinematic calibration.

1. Introduction

At present, hip joint replacement surgery accounts for a large proportion of artificial joint replacement surgeries conducted around the world. Winiarski *et al*. conducted a functional and biomechanical assessment of gait in a patient after bilateral Total Hip Arthroplasty (THA) due to severe degenerative changes in the hip.[1] Any new type of artificial hip joint material must undergo large amounts of material tribology testing before use. Di Puccio *et al*. definited the materials and geometrical properties of artificial hip joints and discussed their friction, lubrication and wear characteristics.[2] The test equipment chosen affects the test accuracy to a large extent. Affatato *et al*. reviewed state-of-the-art hip joint simulators that are currently being applied around the world.[3] Parallel manipulators are used for the simulation of hip joint motion based on its advantages of high stiffness, high accuracy, high speed, strong bearing capacity and complex trajectory capability, and makes up for defects in which the motion simulation and force loading of traditional serial hip joint simulators differ from the actual hip joint motion.[4] Zhao presented a kinematic performance evaluation of a three translational degrees-of-freedom parallel robot from the viewpoint of singularity, isotropy and velocity transmission.[5] Ruiz *et al*. proposed a procedure for the kinematic design of a 3-Prismatic-Revolute-Spherical (PRS) compliant parallel manipulator of three degrees of freedom.[6] Sanchez-Alonso *et al*. conducted a kinematic analysis of a novel 6-DOF parallel manipulator using the non-planar geometry and screw theory.[7] Lu *et al*. proposed a novel 5-DOF parallel manipulator with two composite rotational/linear active legs and introduced its kinematics and statics systematically.[8] Kinematic accuracy is an important performance index in a quality evaluation of a parallel manipulator.

* Corresponding author. E-mail: chgcumt@gmail.com, chg@cumt.edu.cn

Briot *et al*. proposed a simpler method for an accuracy evaluation based on a detailed error analysis of 3-DOF planar parallel robots.[9] Cui *et al*. obtained three error sensitivity indexes to evaluate the kinematic accuracy of a 3-DOF parallel robot manipulator.[10] The demand for high accuracy tasks of parallel manipulators is continuously growing, to the point that designing manipulators granting the prescribed accuracy is becoming a critical issue.

Owing to the effects of manufacturing errors, assembly errors and other factors, there is a deviation between the actual and theoretical structural parameters of parallel manipulators, which results in errors between the actual and theoretical poses (position and orientation) of a parallel manipulator. This makes the kinematic model of a parallel manipulator uncertain, thereby affecting the work accuracy. Fu *et al*. researched a kinematic accuracy problem of a new parallel robot with three legs due to the location of the U joint errors, clearance and driving errors.[11] Chen *et al*. proposed an error modeling methodology to establish an error model of parallel robots with parallelogram structures.[12] Therefore, it is necessary and important to develop an effective and accurate approach to predict the influence of pose errors and improve the kinematic accuracy of a parallel manipulator. At present, there are two main methods for this: one is to improve the manufacturing and assembly accuracy, and the other is to identify and compensate the geometric parameters of parallel manipulators through a kinematic calibration. The former requires high manufacturing and assembly accuracy, which greatly increases the cost of manufacturing, whereas the latter only requires manufacturing machinery components with a certain level accuracy; however, to meet the demand for actual accuracy, a kinematic calibration is used to obtain structural parameters close to reality after the installation is completed. From the standpoint of application, the latter is frequently used in engineering.

A kinematic analysis of parallel manipulators is a necessary procedure prior to establishing an error model. Dumlu *et al*. conducted a kinematic analysis of a 6-DOF RSS parallel manipulator using the D–H method.[13] The pose error calculation model is the foundation of the accuracy analysis and kinematic calibration of a parallel manipulator. Vector and matrix methods are being increasingly used for pose error modeling of parallel manipulators. Bai *et al*. proposed an error source classification method based on a closed loop vector method, which divides geometric errors into two types, namely, compensation and non-compensation errors, and helps with error calibration and compensation.[14] However, with a vector method, it is difficult to describe the relative pose between the rods of compound joints, such as a hook or spherical joint. Therefore, such joints are regarded as ideal joints in modeling, and only the position errors of the joints and the errors of the joint lever lengths are incorporated into the geometric error model, whereas manufacturing errors of the joints are ignored. The matrix method is used to establish an error model that contains more comprehensive error sources based on the D–H matrix. Therefore, the D–H method is commonly used for parallel manipulators, which require high accuracy. Chanal *et al*. studied the influence of an inverse kinematic model on the machining performance of a parallel machine tool, and conducted a quantitative analysis on the manufacturing and assembly errors of the mechanical parts.[15] Chibbi *et al*. analyzed the clearance of the joints and established an error model based on the principle of virtual work; in addition, they analyzed the manipulator errors caused by the clearance of the joints. However, the angle errors of the joints were not involved in their research.[16]

A kinematic calibration is an important research area with regard to the kinematic accuracy of parallel manipulators. Large numbers of studies on calibration have been conducted in recent decades. Sun *et al*. proposed a laser tracker based on kinematic calibration of a 3-DOF rotational parallel manipulator that would be applied in tracking and positioning fields.[17] Fan *et al*. proposed a new calibration approach for a parallel manipulator based on the direct kinematic model and the genetic algorithm.[18] Tian *et al*. presented a simple and effective approach for kinematic calibration of a 3-DOF spindle head developed for high-speed machining.[19] Wang *et al*. investigated a kinematic calibration of a 3-DOF parallel manipulator based on the minimal linear combinations of error parameters.[20] Calibration methods can be divided into two types: self-calibration and external calibration. A self-calibration method is used to obtain measurement information based on internal transducers or external constraints. Chiu *et al*. realized the calibration of a hexapod parallel machine tool by utilizing telescopic rods installed between the base and moving platforms.[21] The disadvantage of a self-calibration method is that it is difficult or even impossible to install transducers on the passive joints (such as the spherical joints) of certain manipulators. An external calibration method is used to detect the terminal pose information through external transducers, and construct the residuals between the measured and calculated values. In addition, geometric parameters are identified through a corresponding

identification model based on inverse or forward kinematics. Ren *et al*. adjusted the pose of a moving platform by installing a biaxial inclinometer and selecting the effective configurations measured under the conditions of attitude constraints to realize a kinematic calibration, and the effectiveness of the method was verified through a simulation and experiment.[22] Bai *et al*. proposed a fuzzy difference calibration method, which simplifies the calibration process and meets the requirement of a small workspace of a parallel manipulator.[23] Zhang *et al*. proposed a comprehensive compensation method for the errors incurred using parallel manipulators. The geometric and thermal errors were assumed to be a single virtual error source based on the theory of virtual error, and a co-existence evolution neural network algorithm was used to realize a compensation of virtual errors.[24]

This paper presents a kinematic accuracy study of a 2(3HUS+S) parallel manipulator for the simulation of hip joint motion, which can be used to test the friction and wear of two artificial hip joints simultaneously, allowing a high test efficiency to be obtained.[25] This type of parallel manipulator is mainly used in medicine to make the artificial hip joint motion correspond to the actual hip joint motion and meet the requirements of hip joint replacement surgery. Research on a parallel hip joint simulator is meaningful for the development of future medical applications. The purpose of this paper is to improve the kinematic accuracy of the manipulator. The remainder of this paper is organized as follows. In Section 2, the prototype and topology of the 2(3HUS+S) parallel manipulator are briefly described. In Section 3, a D–H coordinate system is established, and the kinematic equation of the manipulator is obtained. A D-H transformation matrix is used as the error-modeling tool, and the kinematic error model containing comprehensive manufacturing errors and assembly errors of the manipulator is established based on the perturbation theory. In Section 4, an error equation and an objective function are established. An iterative Levenberg–Marquardt algorithm based on the least squares method is used to uniformly identify the geometric errors in the error model. In addition, error compensation is completed through substituting the identified values into the kinematic model. Based on the actual attitudes of the moving platforms measured during the experiment, the actual kinematic calibration process is simulated through MATLAB software. The effectiveness of the proposed calibration method is verified by comparing the attitude errors after calibration with those before calibration. Finally, our conclusions are presented in Section 5.

2. Manipulator Description

2.1. 2(3HUS+S) parallel manipulator

The topology and prototype distribution of the 2(3HUS+S) parallel manipulator are shown in Fig. 1(a) and (b), respectively. The parallel manipulator is mainly composed of two moving platforms, three linear modules, a base platform and an intermediate branched chain. Each moving platform is connected with the base platform by three identical HUS-type branched chains and an S-type intermediate chain. Every linear module has two sliders with a constant distance between them, which are connected with a corresponding joint lever through a hook joint (U pair). In addition, the other end of the joint lever is connected with the corresponding moving platform through a spherical joint (S pair). The intermediate branched chain is fixed to the base platform at one end and connected with moving platform 2 through a thrust ball bearing at the other end. A ball spline shaft is connected with the artificial hip joint of moving platform 2 at one end, and connected with moving platform 1 through another thrust ball bearing at the other end. The hydraulic cylinder is connected with the artificial hip joint of moving platform 1 through a pressure transducer. The loading force of the hydraulic cylinder acts on the artificial hip joint of moving platform 1 through a guide block and a pressure transducer, and is transmitted to the artificial hip joint of moving platform 2 by a ball spline shaft. The intermediate branched chain is a passive branched chain, which is mainly used for installing artificial hip joints and balancing the loading force of a hydraulic cylinder in the vertical direction. A spring is used to balance the gravity of moving platform 1. Although the loading forces acting on the two artificial hip joints differ, the influence on the experiment results can be ignored. Moving platforms 1 and 2 are driven using three linear modules simultaneously. Therefore, the two moving platforms can obtain identical motion.

As shown in Fig. 1(a), a_{ji} and b_{ji} ($i = 1, 2, 3$; $j = 1, 2$) are the installation positions of the spherical joint on the moving platform and the hook joint on the slider, respectively. In addition, A_i is the installation position of the linear module on the base platform; c_i is the projection point of b_{1i}

https://doi.org/10.1017/S0263574718000073 Published online by Cambridge University Press

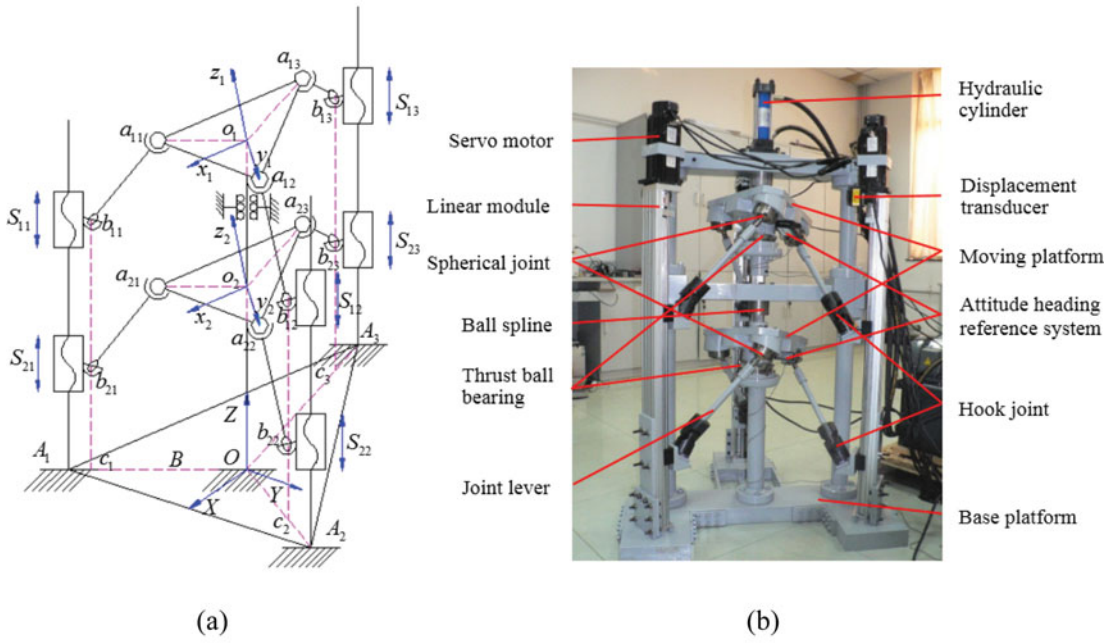

Fig. 1. 2(3HUS+S) parallel manipulator for simulation of hip joint motion. (a) Topology of the manipulator. (b) Prototype of the manipulator.

and b_{2i} on OA_i; and o_1, o_2, and O are the centers of the triangles $a_{11}a_{12}a_{13}$, $a_{21}a_{22}a_{23}$, and $A_1A_2A_3$, respectively. The absolute coordinate system O-XYZ is set up on the base platform. The coordinate system takes point O as the origin, the negative direction of the X-axis passes through point A_3, the Z-axis is perpendicular to the base platform and points to the moving platform, and the Y-axis is determined based on the right-hand rule. The relative coordinate system o_j-$x_jy_jz_j$ is set up on the moving platform. The coordinate system takes point o_j as the origin, the y_j-axis passes through point a_{j3}, and the z_j-axis is perpendicular to the moving platform and points toward the outside. The orientations of the x_j-axis, y_j-axis and z_j-axis follow the right-hand rule. The spherical joints are installed symmetrically on the moving platforms around the origin of the corresponding coordinate system o_j-$x_jy_jz_j$. The linear modules are installed symmetrically on base platform B around the origin of the coordinate system O-XYZ. The spatial attitudes of the two moving platforms are determined based on the displacement of the sliders.

2.2. Degrees of freedom

According to the revised Kutzbach–Grubler formula, the degrees of freedom of the manipulator can be given by

$$M = d(n - g - 1) + \sum_{i=1}^{g} f_i + v - \zeta \tag{1}$$

where d is the order of the manipulator, $d = 6$; n is the number of components, $n = 8$; g is the number of all motion pairs, $g = 10$; f_i is the number of relative degrees of freedom for the ith motion pair, $\sum_{i=1}^{g} f_i = 21$; v is the number of redundant constraints, $v = 0$; and ζ is the number of the local degrees of freedom, $\zeta = 0$. Substituting these parameter values into Eq. (1), $M = 6 \times (8\text{-}10\text{-}1) + 21 + 0 - 0 = 3$ can be obtained.

Therefore, the 2(3HUS+S) parallel manipulator has three degrees of freedom. After the manipulator is given a certain amount of preload using the hydraulic cylinder, it has no translation in the three directions. According to the above analysis, the three degrees of freedom of the manipulator are all rotations. That is, the 2(3HUS+S) parallel manipulator has three rotational degrees of freedom.

https://doi.org/10.1017/S0263574718000073 Published online by Cambridge University Press

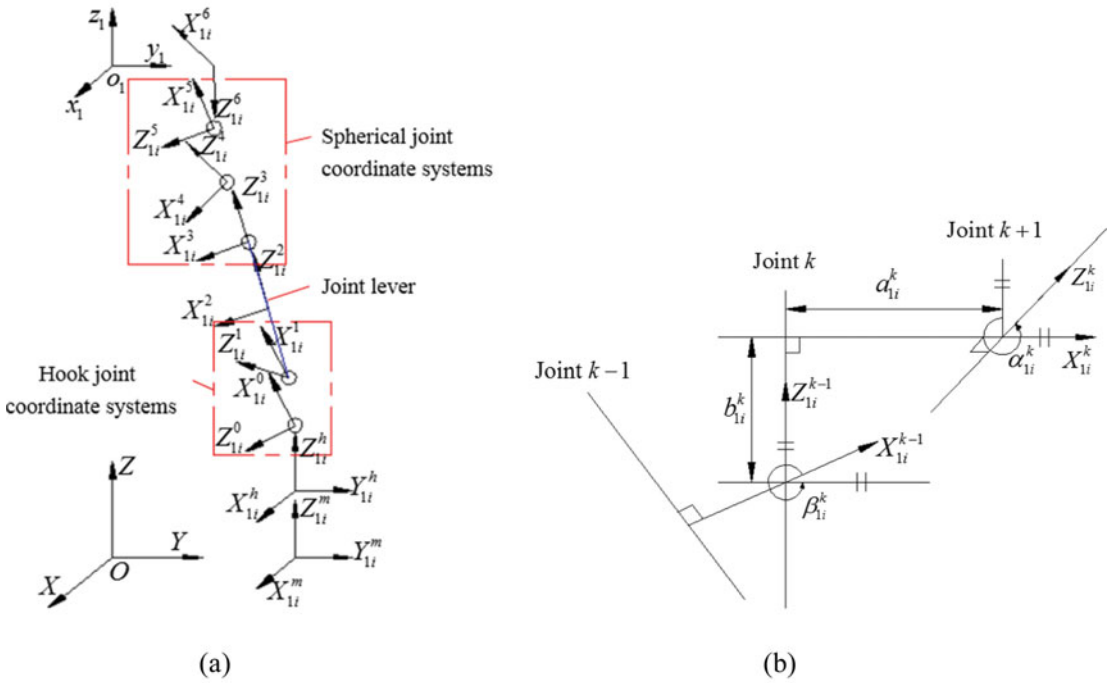

Fig. 2. D–H coordinate system and D–H parameters of 2(3HUS+S) parallel manipulator. (a) D–H coordinate system. (b) D–H parameters of the rotation joint links.

3. Kinematic Error Modeling

3.1. Kinematic model

The kinematic model is established using the D–H method. In the kinematic analysis, each HUS-type branched chain of the 2(3HUS+S) parallel manipulator can be transformed into an H–2R–3R type branched chain. Assume that each branched chain of the parallel manipulator is a single-opened chain. Because the configuration of the kinematic pair for each branched chain is identical, the D–H coordinate system of the branched chain with moving platform 1 is established according to the postposition of the fixed coordinate system. Schematic diagrams of the D–H coordinate system and the D–H parameters of the rotation joint links are shown in Fig. 2(a) and (b), respectively.

The local coordinate system (k-system) fixed on the kth rod ($k = 1$–6) in the branched chain is established, as shown in Fig. 2(a). The rod length, torsional angle, rod distance and rotational angle are the D–H parameters relating to the kth rod, and are defined as a_{1i}^k, α_{1i}^k, b_{1i}^k and β_{1i}^k ($k = 1$–6, $i = 1$, 2, 3), respectively. In each branched chain, the rod length a_{1i}^k and torsional angle α_{1i}^k are the geometric parameters of the rods, and remain constant. The rod distance b_{1i}^k or joint lever length l_{1i} is constant, and the rotational angle is the motion parameter of the driven joints and changes in real time. The pose transformation matrix between adjacent rods is described as

$$\boldsymbol{T}_{1i}^{k-1,k} = \mathrm{Rot}(Z_{1i}^{k-1}, \beta_{1i}^k)\mathrm{Trans}(0, 0, b_{1i}^k)\mathrm{Trans}(a_{1i}^k, 0, 0)\mathrm{Rot}(X_{1i}^k, \alpha_{1i}^k) \quad k = 1-6, i = 1,\ 2,\ 3 \quad (2)$$

where Rot represents a homogeneous rotation transformation and Trans indicates a homogeneous translation transformation.

The coordinate system (m-system) of point c_i in Fig. 1(a) is fixed on the base platform, and the relative pose between the m-system and base platform coordinate system (O-system) is determined through the following transformation. Initially, the m-system coincides with the O-system. First, the m-system translates along the X- and Y-axes, and the distances of the translation are $r_b\cos\beta_{Oi}$ and $r_b\sin\beta_{Oi}$, respectively. Then, the m-system rotates ($\beta_{Oi} - \pi/2$) around the Z_{1i}^m-axis, and the origin of the m-system reaches point c_i. The transformation matrix from the O-system to the m-system can be

https://doi.org/10.1017/S0263574718000073 Published online by Cambridge University Press

expressed as

$$\boldsymbol{T}_{1i}^{Om} = \text{Trans}(r_b cos\beta_{Oi}, r_b sin\beta_{Oi}, 0)\text{Rot}(Z_{1i}^{m}, \beta_{Oi} - \pi/2) \quad (i = 1,\ 2,\ 3) \tag{3}$$

where r_b is the distance from the center of the hook joints to the Z-axis, and β_{Oi} is the distribution angle of the linear modules on the base platform.

The relative pose between the coordinate system (h-system) of the slider and the m-system is determined through the following transformation. Initially, the h-system coincides with the m-system. Then, the m-system translates along the Z_{1i}^{m}-axis, the distance of the translation is L_{1i} and the origin of the h-system reaches point b_{1i}. The transformation matrix from the O-system to the m-system is obtained as

$$\boldsymbol{T}_{1i}^{mh} = \text{Trans}(0, 0, L_{1i}) \quad (i = 1,\ 2,\ 3) \tag{4}$$

where L_{1i} is the displacement of the sliders.

The relative pose between the coordinate system (0−system) of the hook joint bearing and the h-system is determined through the following transformation. Initially, the 0−system coincides with the h-system. Then, the 0−system rotates $\pi/2$, $\pi/2$ and $-\pi/6$ around the X_{1i}^{0}-axis, Z_{1i}^{0}-axis and Y_{1i}^{0}-axis, respectively. The position at the moment is the location of the 0-system. The transformation matrix from the h-system to the 0-system is obtained as

$$\boldsymbol{T}_{1i}^{h0} = \text{Rot}\left(X_{1i}^{0}, \frac{\pi}{2}\right)\text{Rot}\left(Z_{1i}^{0}, \frac{\pi}{2}\right)\text{Rot}\left(Y_{1i}^{0}, -\frac{\pi}{6}\right) \quad (i = 1,\ 2,\ 3) \tag{5}$$

The coordinate system (6−system) of the spherical joint is fixed on the moving platform, and the relative pose between the 6−system and the moving platform coordinate system (o_1-system) is determined through the following transformation. Initially, the o_1-system coincides with the 6−system. First, the o_1-system rotates π and $(\pi/2-\alpha_{oi})$ around the y_1-axis and z_1-axis, respectively. Then, the o_1-system translates along the x_1-axis and y_1-axis, the distances of the translation are $-r_a\cos\alpha_{oi}$ and $-r_a\sin\alpha_{oi}$, respectively, and the origin of the o_1−system reaches point o_1. The transformation matrix from the 6-system to the o_1-system is written as

$$\boldsymbol{T}_{1i}^{6o_1\prime} = \text{Rot}(y_1, \pi)\text{Rot}(z_1, \pi/2 - \alpha_{oi})\text{Trans}(-r_a\cos\alpha_{oi}, -r_a\sin\alpha_{oi}, 0) \quad (i = 1,\ 2,\ 3) \tag{6}$$

where r_a is the installation radius of the spherical joints on the moving platform and α_{oi} is the distribution angle of the spherical joints.

According to the above analysis, the kinematic equation of branch $1i$ is given by

$$\boldsymbol{T}_{1i}^{Oo_1} = \boldsymbol{T}_{1i}^{Om}\boldsymbol{T}_{1i}^{mh}\boldsymbol{T}_{1i}^{h0}\boldsymbol{T}_{1i}^{01}\boldsymbol{T}_{1i}^{12}\boldsymbol{T}_{1i}^{23}\boldsymbol{T}_{1i}^{34}\boldsymbol{T}_{1i}^{45}\boldsymbol{T}_{1i}^{56}\boldsymbol{T}_{1i}^{6o_1} \quad (i = 1,\ 2,\ 3) \tag{7}$$

where $\boldsymbol{T}_{1i}^{Oo_1}$ is the pose transformation matrix of moving platform 1 relative to the base platform.

3.2. Error model

The error model established through a vector method only includes the position errors of the joints and the sliders and the errors of the joint lever lengths, whereas the motion of the joints cannot be reflected in the model. However, the error model established using the D–H method can include manufacturing errors of the joints, which can reflect the error sources affecting the kinematic accuracy of the manipulator in a comprehensive manner. Therefore, the error model is established using the D–H method based on the perturbation theory. First, the error parameters are introduced. Obviously, in addition to the motion parameters of the driven joints, the D–H parameters of the rods are the structural parameters of the branched chains. These parameters are collectively referred to as the geometric parameters. The errors in the geometric parameters caused by the manufacturing and assembly are known as geometric errors. Assume that the influence of non-geometric errors on an error in attitude is much smaller than that of geometric errors, and can therefore be ignored owing to the high stiffness of a parallel manipulator. The actual D–H parameters of the 2(3HUS+S) parallel manipulator are shown in Table I.

https://doi.org/10.1017/S0263574718000073 Published online by Cambridge University Press

Table I. Actual D–H parameters of 2(3HUS+S) parallel manipulator.

Numbers	$a_{1i}^{k\prime}$ (mm)	$\alpha_{1i}^{k\prime}$ (°)	$b_{1i}^{k\prime}$ (mm)	$\beta_{1i}^{k\prime}$ (°)
1	δa_{1i}^{1}	$-\pi/2+\delta\alpha_{1i}^{1}$	0	β_{1i}^{1}
2	δa_{1i}^{2}	$-\pi/2+\delta\alpha_{1i}^{2}$	0	β_{1i}^{2}
3	δa_{1i}^{3}	$\delta\alpha_{1i}^{3}$	$l_{1i}+\delta l_{1i}$	0
4	δa_{1i}^{4}	$\pi/2+\delta\alpha_{1i}^{4}$	0	β_{1i}^{4}
5	δa_{1i}^{5}	$\pi/2+\delta\alpha_{1i}^{5}$	0	β_{1i}^{5}
6	0	$-7\pi/18$	0	β_{1i}^{6}

In Table I, $a_{1i}^{k\prime}$, $\alpha_{1i}^{k\prime}$, $b_{1i}^{k\prime}$, and $\beta_{1i}^{k\prime}$ ($k = 1$–6; $i = 1, 2, 3$) represent the actual rod length, torsional angle, rod distance and rotational angle of the manipulator during motion, respectively. In addition, δa_{1i}^{k} and $\delta\alpha_{1i}^{k}$ are the offset error and angle error between the adjacent rotation axes, respectively.

The actual pose matrix between the adjacent rods in the rod coordinate systems is

$$\boldsymbol{T}_{1i}^{k-1,k} = \mathrm{Rot}(Z_{1i}^{k-1},\ \beta_{1i}^{k\prime})\mathrm{Trans}(0,0,b_{1i}^{k\prime})\mathrm{Trans}(a_{1i}^{k\prime},0,0)\mathrm{Rot}(X_{1i}^{k},\alpha_{1i}^{k\prime}) \quad k = 1-6,\ i = 1,\ 2,\ 3 \tag{8}$$

The position errors of the sliders, δL_{11}, δL_{12} and δL_{13}; the errors of the joint lever lengths, δl_{11}, δl_{12} and δl_{13}; the installation position errors of the spherical joints, δr_{a1ix}, δr_{a1iy} and δr_{a1iz} ($i = 1, 2, 3$); the installation position errors of the hook joints, δr_{b1ix}, δr_{b1iy} and δr_{b1iz} ($i = 1, 2, 3$); the installation position errors of moving platform 1, δX_{o1}, δY_{o1} and δZ_{o1}; the distribution angle errors of the spherical joints on moving platform 1, δb_{1i} ($i = 1, 2, 3$) and the distribution angle errors of the linear modules on the base platform, δd_i ($i = 1, 2, 3$) are taken into account in the error model, in addition to the errors of the D–H parameters. According to the actual transformation matrix between the rod coordinate systems, the errors transformation matrix from the absolute coordinate system *O-XYZ* to the relative coordinate system o_1-$x_1y_1z_1$ can be obtained based on the perturbation theory.

$$\boldsymbol{T}_{1i}^{Oo_1\prime} = \boldsymbol{T}_{1i}^{Om\prime}\boldsymbol{T}_{1i}^{mh\prime}\boldsymbol{T}_{1i}^{h0\prime}\boldsymbol{T}_{1i}^{01\prime}\boldsymbol{T}_{1i}^{12\prime}\boldsymbol{T}_{1i}^{23\prime}\boldsymbol{T}_{1i}^{34\prime}\boldsymbol{T}_{1i}^{45\prime}\boldsymbol{T}_{1i}^{56\prime}\boldsymbol{T}_{1i}^{6o_1\prime} = \begin{bmatrix}\boldsymbol{R}_{1i}^{Oo_1\prime} & \boldsymbol{P}_{1i}^{Oo_1\prime}\\ 0 & 1\end{bmatrix} \quad (i = 1, 2, 3) \tag{9}$$

where

$$\begin{aligned}\mathbf{T}_{1i}^{Om\prime} = {}&\mathrm{Trans}(r_b cos(\beta_{Oi}+\delta d_i)+\delta r_{b1ix}, r_b sin(\beta_{Oi}+\delta d_i)+\delta r_{b1iy}, \delta r_{b1iz})\\ &\times \mathrm{Rot}(Z_{1i}^{m}, \beta_{Oi}+\delta d_i-\pi/2)\,(i = 1, 2, 3)\end{aligned} \tag{10}$$

$$\boldsymbol{T}_{1i}^{mh\prime} = \mathrm{Trans}(0, 0, L_{1i}+\delta L_{1i}) \quad (i = 1,\ 2,\ 3) \tag{11}$$

$$\boldsymbol{T}_{1i}^{h0} = \mathrm{Rot}\left(X_{1i}^{0}, \frac{\pi}{2}\right)\mathrm{Rot}\left(Z_{1i}^{0}, \frac{\pi}{2}\right)\mathrm{Rot}\left(Y_{1i}^{0}, -\frac{\pi}{6}\right) \quad (i = 1,\ 2,\ 3) \tag{12}$$

$$\begin{aligned}&\boldsymbol{T}_{1i}^{6o_1\prime} = \mathrm{Rot}(y_1,\pi)\mathrm{Rot}(z_1,\pi/2-\alpha_{oi}-\delta b_i)\mathrm{Trans}(-r_{a1}\cos(\alpha_{oi}+\delta b_i)-\delta r_{a1ix},\\ &-r_{a1}\sin(\alpha_{oi}+\delta b_i)-\delta r_{a1iy}, -\delta r_{a1iz})\,(i = 1, 2, 3)\end{aligned} \tag{13}$$

The actual pose matrix of moving platform 1 can be obtained by utilizing the pose transformation directly.

$$\begin{aligned}\boldsymbol{T}'_1 = \begin{bmatrix}\boldsymbol{R}'_1 & \boldsymbol{P}'_1\\ 0 & 1\end{bmatrix} = {}&\mathrm{Trans}\,(\delta X_{o1}+\delta X_{o2}, \delta Y_{o1}+\delta Y_{o2}, h_1+\delta Z_{o1}+\delta Z_{o2})\\ &\times \mathrm{Rot}(Z,\gamma')\mathrm{Rot}(Y,\beta')\mathrm{Rot}(X,\alpha') \quad (i = 1,\ 2,\ 3)\end{aligned} \tag{14}$$

where $\boldsymbol{R}_1$'is the actual attitude matrix of moving platform 1, $\boldsymbol{P}_1$' is the position vector of the o_1-system origin in the *O*-system and h_1 is the theoretical installation height. The position vector of

https://doi.org/10.1017/S0263574718000073 Published online by Cambridge University Press

moving platform 1 is affected by the installation position errors of moving platform 2, δX_{o2}, δY_{o2} and δZ_{o2}, which is due to moving platform 1 being fixed over the rotation center of moving platform 2 in series through a ball spline shaft. In addition, $\delta X_{o1} + \delta X_{o2}$, $\delta Y_{o1} + \delta Y_{o2}$, $h_1 + \delta Z_{o1} + \delta Z_{o2}$, α', β' and γ' are the actual pose parameters of the manipulator.

The relationship between the geometric errors of branch $1i$ and the actual pose parameters of moving platform 1 can be established according to the above analysis.

$$\boldsymbol{T}_{1i}^{Oo_1'} = \boldsymbol{T}'_1 \quad (i = 1,\ 2,\ 3) \tag{15}$$

Similarly, the relationship between the geometric errors of other branches and the actual pose parameters of the moving platform can be obtained. The actual pose of the moving platform can be solved by substituting the displacement values of the sliders under the theoretical pose and all error values into Eq. (15), and the pose error can then be obtained. Therefore, the establishment of the error model is completed. The error model reflects the error sources affecting the kinematic accuracy of the parallel manipulator more comprehensively, which provides the theoretical basis for the identification of the geometric errors and facilitates the realization of the accurate error compensation in the kinematic calibration of the manipulator.

4. Kinematic Calibration

4.1. Calibration method

Here, $\boldsymbol{R}_{1i}^{Oo_1'} = \boldsymbol{R}'_1$ and $\boldsymbol{P}_{1i}^{Oo_1'} = \boldsymbol{P}'_1$ can be obtained owing to $\boldsymbol{T}_{1i}^{Oo_1'} = \boldsymbol{T}'_1$. A total of 12 equations can be established for each branched chain, and therefore six branches can result in 72 equations, and 72 unknowns can be solved. These 72 equations can be expressed through the following functional form:

$$\begin{cases} f_1 = \boldsymbol{T}_{11}^{Oo_1'}(1,1) - \boldsymbol{T}'_1(1,1) \\ f_2 = \boldsymbol{T}_{11}^{Oo_1'}(1,2) - \boldsymbol{T}'_1(1,2) \\ \cdots \\ f_{36} = \boldsymbol{T}_{13}^{Oo_1'}(3,4) - \boldsymbol{T}'_1(3,4) \\ \cdots \\ f_{72} = \boldsymbol{T}_{23}^{Oo_1'}(3,4) - \boldsymbol{T}'_2(3,4) \end{cases} \tag{16}$$

There are 123 unknowns in the above equations, which include the geometric errors related to moving platform 2: the offset errors between the rotation axes, δa_{2i}^k ($i = 1, 2, 3$, $k = 1$–5); the angle errors between the rotation axes, $\delta\alpha_{2i}^k$ ($i = 1, 2, 3$, $k = 1$–5); the position errors of the sliders, δL_{21}, δL_{22} and δL_{23}; the errors of the joint lever lengths, δl_{21}, δl_{22} and δl_{23}; the installation position errors of the spherical joints, δr_{a2ix}, δr_{a2iy} and δr_{a2iz} ($i = 1, 2, 3$); the installation position errors of the hook joints, δr_{b2ix}, δr_{b2iy} and δr_{b2iz} ($i = 1, 2, 3$) and the distribution angle errors of the spherical joints on moving platform 2, δb_{2i} ($i = 1, 2, 3$). Thirty-six equations can be obtained through each measured attitude of the moving platform; therefore, at least four groups of suitable attitudes need to be measured. The errors can be solved using the least squares method after a sufficient number of attitudes are measured. Assume that 20 groups of moving platform attitudes and slider displacement are measured, the objective function can be established as

$$\boldsymbol{F} = \min \sum_{m=1}^{20} \sum_{n=1}^{36} (f_n)^2 \tag{17}$$

Assume that

$$\varepsilon = [\delta L_{ji}, \delta l_{ji}, \delta r_{ajix}, \delta r_{ajiy}, \delta r_{ajiz}, \delta r_{bjix}, \delta r_{bjiy}, \delta r_{bjiz}, \delta X_{oj}, \delta Y_{oj}, \delta Z_{oj}, \delta b_{ji}, \delta d_i, \delta a_{ji}{}^1, \delta a_{ji}{}^2, \delta a_{ji}{}^3,$$
$$\times \delta a_{ji}{}^4, \delta a_{ji}{}^5, \delta\alpha_{ji}{}^1, \delta\alpha_{ji}{}^2, \delta\alpha_{ji}{}^3, \delta\alpha_{ji}{}^4, \delta\alpha_{ji}{}^5]^{\mathrm{T}}\ (j = 1,\ 2;\ i = 1,\ 2,\ 3),\ f = \left[f_1, f_2, \ \ldots, f_{720}\right]^{\mathrm{T}}.$$

https://doi.org/10.1017/S0263574718000073 Published online by Cambridge University Press

Table II. Geometric parameters of 2(3HUS+S) parallel manipulator.

Geometric parameters	Values	Geometric parameters	Values
Length of the joint levers l_{ji} (mm)	328	Installation height of moving platform 1 h_1 (mm)	899
Installation radius of the spherical joints r_a (mm)	144	Installation height of moving platform 2 h_2 (mm)	490
Distance from the center of the hook joints to the Z-axis r_b (mm)	265	Allowable rotation angle of the spherical joints (°)	30

The error equation can be written as

$$f(\boldsymbol{\varepsilon}) = 0 \tag{18}$$

Equation (18) is a non-linear equation and is difficult to solve. Therefore, a linear equation is obtained through a linearization method. A Taylor series expansion is used for Eq. (18), where the high-order remainder is omitted, and Eq. (19) can be obtained by regarding $\boldsymbol{\epsilon}_0 = 0$ as the approximation vector of the errors.

$$f(\boldsymbol{\varepsilon}_0) + \frac{\partial f(\boldsymbol{\varepsilon})}{\partial \boldsymbol{\varepsilon}}|_{\varepsilon=\varepsilon_0} \cdot \Delta\boldsymbol{\varepsilon} = 0 \tag{19}$$

To avoid singular matrix, the iterative Levenberg–Marquardt algorithm based on the least squares is used to solve Eq. (19).

Assume that $\boldsymbol{E} = \frac{\partial f(\boldsymbol{\varepsilon})}{\partial \boldsymbol{\varepsilon}}$, then

$$\Delta\boldsymbol{\varepsilon} = -[(\boldsymbol{E}^T\boldsymbol{E} + \lambda\boldsymbol{I})^{-1}\boldsymbol{E}^T]f(\boldsymbol{\varepsilon}) \tag{20}$$

where λ is the modifying factor of the Levenberg–Marquardt algorithm.

$$\boldsymbol{\varepsilon}_{s+1} = \boldsymbol{\varepsilon}_s + \Delta\boldsymbol{\varepsilon} \tag{21}$$

Equation (21) is a modifying equation of a geometric error vector in the calibration, and $\boldsymbol{\epsilon}$ is modified through a continuous iteration. The iteration is completed once the geometric errors make the objective function sufficiently small, and the optimal solution of the geometric errors can be obtained.

A calibration algorithm flow chart of the 2(3HUS+S) parallel manipulator is shown in Fig. 3.

The identification values of the geometric errors are substituted into the kinematic model in the control software to realize the error compensation. The theoretical attitudes after compensation can be obtained through forward kinematics. The attitude errors of the moving platforms can be obtained by comparing the measured values with the theoretical values. Therefore, the kinematic calibration of the manipulator is completed.

4.2. Results of calibration and simulation

A 2(3HUS+S) parallel manipulator is shown in Fig. 1, the geometric parameters of which are shown in Table II.

According to ISO14242-1:2002(E) artificial hip joint prosthesis test standard, the operation frequency of a friction and wear test for a hip joint prosthesis is 1 HZ ± 0.1 HZ, and the range of motion angle for flexion/extension (FE), abduction/adduction (AA) and internal/external rotation (IER) are −18–25°, −4–7° and −10–2°, respectively. The Z-, X- and Y-axes are defined as the rotation axes of the FE, AA and IER, respectively. According to the actual motion trajectory of an artificial hip joint, the motion law of the moving platforms for the 2(3HUS+S) parallel manipulator is shown

https://doi.org/10.1017/S0263574718000073 Published online by Cambridge University Press

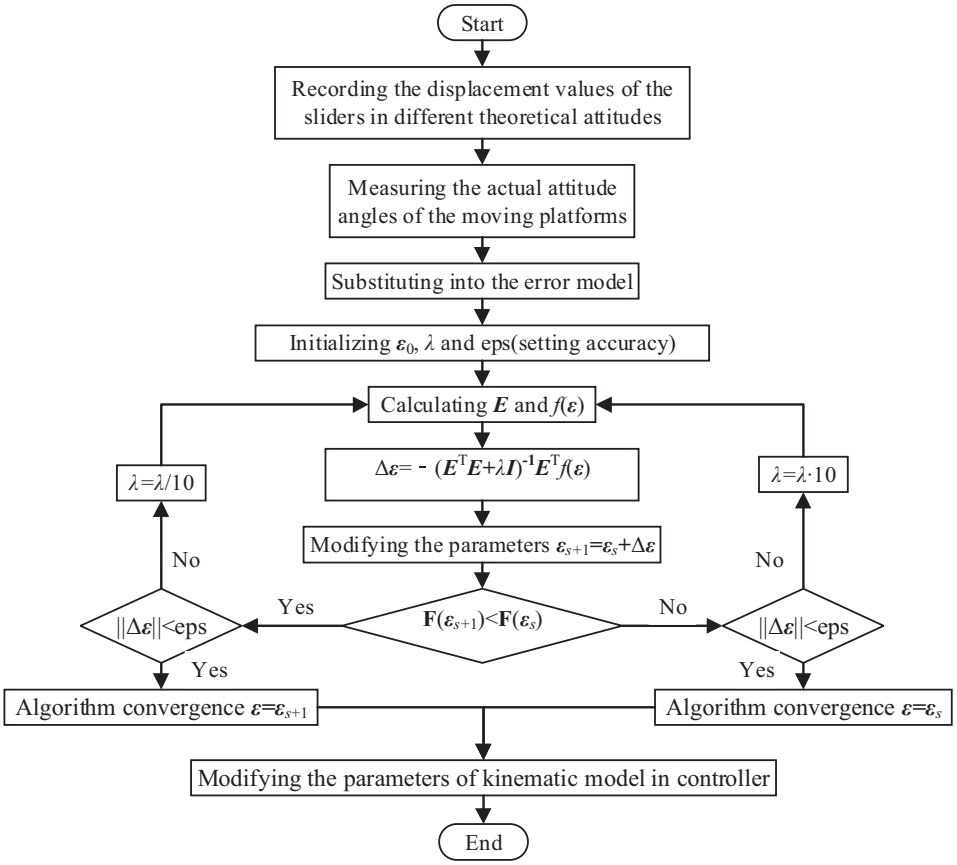

Fig. 3. Calibration algorithm flow chart of 2(3HUS+S) parallel manipulator.

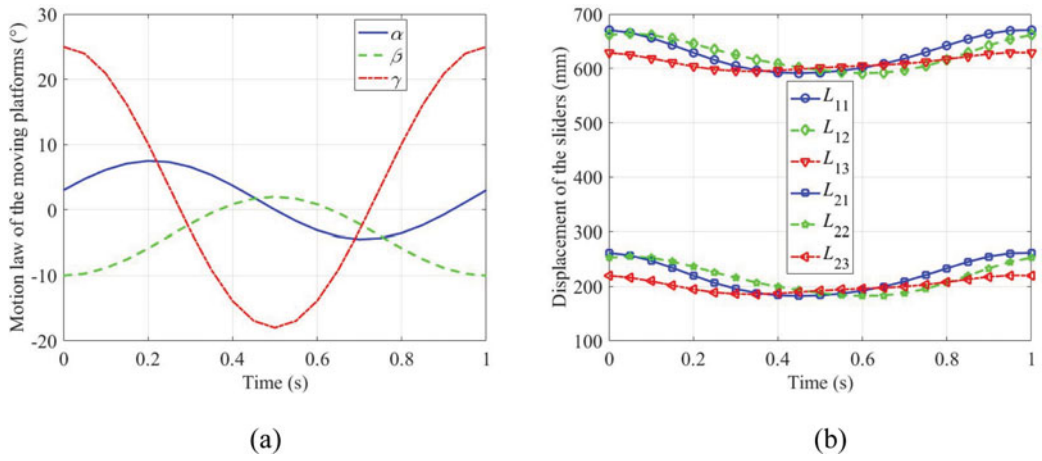

Fig. 4. Test parameters of 2(3HUS+S) parallel manipulator. (a) Motion trajectory of the moving platforms. (b) Displacement of the sliders.

in Fig. 4(a), and the mathematics equation is

$$\begin{cases} \alpha = \dfrac{5.5\pi}{180}\cos[2\pi(t-0.21)] + \dfrac{1.5\pi}{180} \\ \beta = \dfrac{6\pi}{180}\cos(2\pi t+\pi) - \dfrac{4\pi}{180} \\ \gamma = \dfrac{21.5\pi}{180}\cos(2\pi t) + \dfrac{3.5\pi}{180} \end{cases} \tag{22}$$

https://doi.org/10.1017/S0263574718000073 Published online by Cambridge University Press

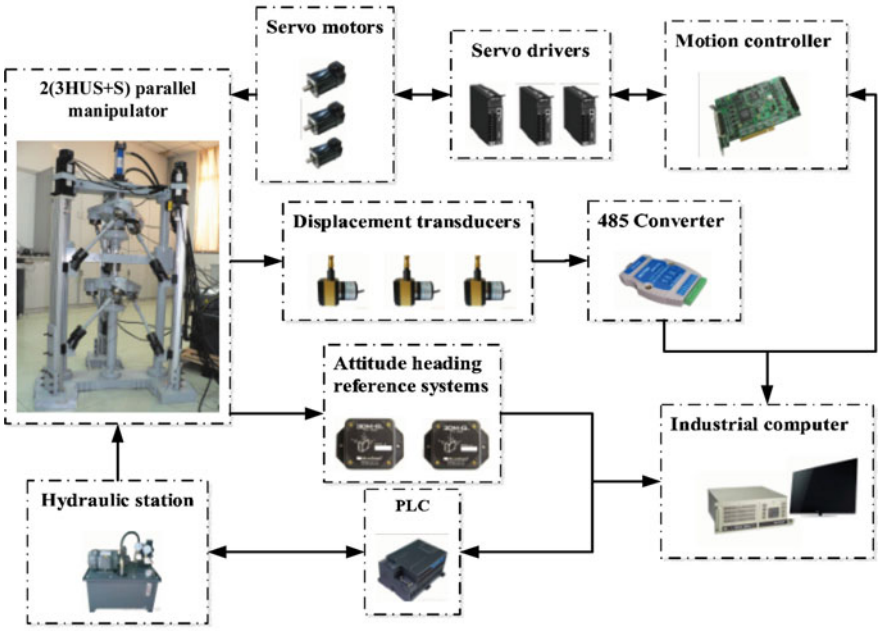

Fig. 5. Experiment diagram of 2(3HUS+S) parallel manipulator.

where t is the driving time, and α, β and γ are the rotation angles of the moving platforms around the X-, Y- and Z-axes, respectively.

The displacement value of each slider can be calculated through the inverse kinematics based on the motion trajectory of the moving platforms and the kinematic model. The displacement curves of the sliders driven by the linear modules are obtained, as shown in Fig. 4(b).

To verify the proposed kinematic calibration method, a simulation experiment of the 2(3HUS+S) parallel manipulator is carried out in a laboratory. The control system of the manipulator is mainly composed of an industrial computer, a motion controller (GTS-400), three displacement transducers (CESI-S1000P), and two attitude heading reference systems (MPU6050). An experiment diagram is shown in Fig. 5. The attitude heading reference systems are fixed on the moving platforms, which are used to measure the attitudes of the moving platforms. The inverse kinematic model of the manipulator is solved using software in an industrial computer. The industrial computer is applied to send a control signal to the motion controller and receive the information from the displacement transducers and the attitude heading reference systems. The feedback signals of the control system are obtained through the encoder on the servo motors. The loading force from the hydraulic cylinder is controlled using the PLC.

The manipulator is regular in motion according to the displacement of the sliders, as shown in Fig 4(b). In the process of motion, the actual attitudes of the moving platforms are measured based on the attitude heading reference systems fixed on the moving platforms. To obtain accurate calibration results, for each moving platform, 10 groups of measured attitudes in 1 s are selected. Five repeatable experiments and measurements are carried out, and the range of repeatability of the attitude values is 0.001–0.005°. The mean value of the measured attitudes for each group, and each part of the structural parameters of the moving platforms, are substituted into the calibration model. Based on the calibration method proposed in this paper, the numerical simulation is realized using MATLAB software. The calculation time of the calibration algorithm is about 20 min, and the number of iterations is 7. Eventually, the 123 geometric errors identified are as shown in Fig. 6 and Table III.

To express the identification values of different geometric errors in a convenient manner and make the identified geometric errors more intuitive and clear, the identification results are presented in Fig. 6 and Table III, respectively. Furthermore, the position and angle errors are shown in Fig. 6(a) and (b), respectively. It can be seen from the identification values of the geometric errors in Fig. 6(a) and Table III that δr_{bj1x}, δr_{bj2x}, δr_{bj2y}, δr_{bj3y}, δr_{aj2x}, δa^4_{j2} and δa^5_{j2} ($j = 1, 2$) are larger than the other geometric errors. The results show that larger position errors mainly occur in the installation of the

https://doi.org/10.1017/S0263574718000073 Published online by Cambridge University Press

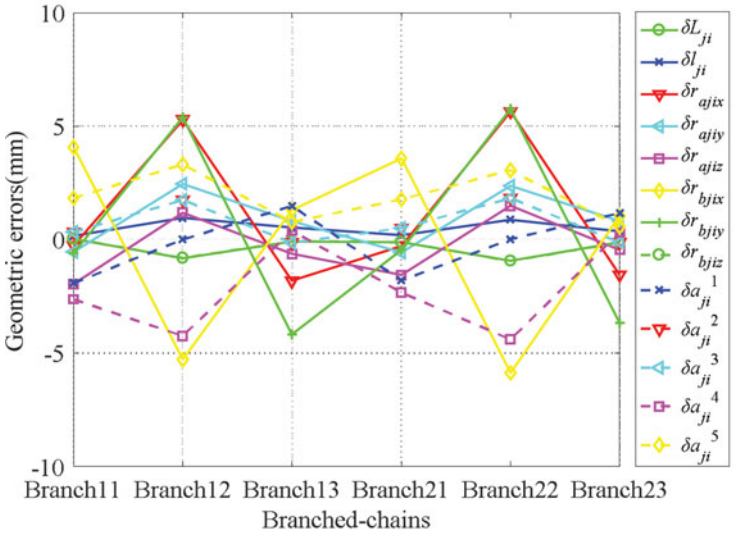

(a)

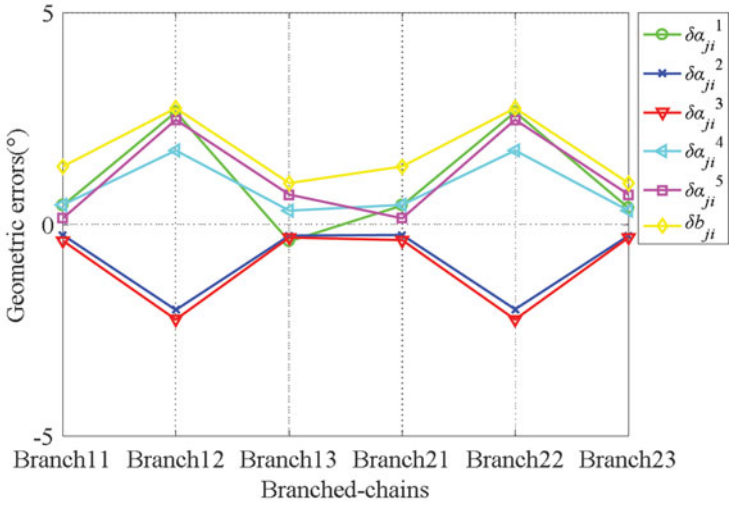

(b)

Fig. 6. Geometric error identification values of 2(3HUS+S) parallel manipulator. (a) Geometric errors-1. (b) Geometric errors-2.

hook joints, the installation of spherical joint a_{j2} and the offset between the rotation axes of spherical joint a_{j2}. Combining Fig. 6(b) with Table III, we can see that $\delta\alpha_{j2}^{1}$, $\delta\alpha_{j2}^{2}$, $\delta\alpha_{j2}^{3}$, $\delta\alpha_{j2}^{4}$, $\delta\alpha_{j2}^{5}$ and δb_{j2} are larger than the other geometric errors. The results show that the larger angle errors mainly occur in the angle between the rotation axes of spherical joint a_{j2} and hook joint b_{j2}, and the distribution angle of spherical joints a_{j2}. Therefore, to reduce the influence of errors in the attitude of the moving platforms and improve the kinematic accuracy of the manipulator, the coordinate error control of the hook joints and spherical joint a_{j2} should be given more attention in the process of assembling the parallel manipulator. In addition, the manufacturing accuracy of both the spherical joints and the hook joints should be improved.

Error compensation is realized by substituting the identified geometric errors into the control model, and the theoretical attitudes after compensation are obtained through forward kinematics. The 10 groups of theoretical attitudes, the actual attitudes, and the attitudes after compensation of the moving platforms are listed in Table IV. The attitude errors of the moving platforms after calibration

https://doi.org/10.1017/S0263574718000073 Published online by Cambridge University Press

Table III. Geometric error identification values of 2(3HUS+S) parallel manipulator.

	Branch11 ($j=1, i=1$)	Branch12 ($j=1, i=2$)	Branch13 ($j=1, i=3$)	Branch21 ($j=2, i=1$)	Branch22 ($j=2, i=2$)	Branch23 ($j=2, i=3$)
$\delta d_i(^\circ)$	−0.1123	−1.7557	−0.2997	/	/	/
δX_{oj}(mm)		0.9112			2.1747	
δY_{oj}(mm)		−0.6370			−2.2655	
δZ_{oj}(mm)		0.8525			2.0218	

Table IV. Attitude data of moving platforms.

	Theoretical attitudes (°)			Actual attitudes (°)			After compensations (°)		
Moving platform 1	α	β	γ	$\alpha 1$	$\beta 1$	$\gamma 1$	$\alpha 1'$	$\beta 1'$	$\gamma 1'$
1	3	−10	25	2.980	−9.875	24.95	3.005	−9.873	24.92
2	6.131	−8.854	20.89	6.247	−8.653	20.41	6.236	−8.627	20.40
3	7.496	−5.854	10.14	7.507	−5.585	9.354	7.507	−5.585	9.354
4	6.574	−2.146	−3.144	6.471	−1.899	−4.085	6.481	−1.902	−4.081
5	3.717	0.8541	−13.89	3.538	1.043	−14.85	3.538	1.016	−14.85
	Theoretical attitudes (°)			Actual attitudes (°)			After compensations (°)		
Moving platform 2	α	β	γ	$\alpha 2$	$\beta 2$	$\gamma 2$	$\alpha 2'$	$\beta 2'$	$\gamma 2'$
1	3	−10	25	2.980	−9.875	24.96	3.005	−9.873	24.93
2	6.131	−8.854	20.89	6.247	−8.653	20.45	6.236	−8.627	20.44
3	7.496	−5.854	10.14	7.507	−5.585	9.415	7.507	−5.585	9.412
4	6.574	−2.146	−3.144	6.471	−1.888	−3.987	6.481	−1.902	−3.988
5	3.717	0.8541	−13.89	3.537	1.043	−14.68	3.538	1.016	−14.69

Table V. Absolute maximum and absolute mean values of attitude errors before and after calibration.

	Absolute maximum values				Absolute mean values			
	Moving platform 1		Moving platform 2		Moving platform 1		Moving platform 2	
Attitude errors	Before	After	Before	After	Before	After	Before	After
$\delta\alpha(^\circ)$	0.1805	0.0331	0.1804	0.0320	0.1020	0.0141	0.1022	0.0143
$\delta\beta(^\circ)$	0.2690	0.0269	0.2690	0.0268	0.1330	0.0142	0.1341	0.0154
$\delta\gamma(^\circ)$	1.1700	0.0556	0.8430	0.0616	0.5907	0.0210	0.5322	0.0254

can be obtained by comparing the theoretical attitudes after compensation with the measured attitudes. The attitude errors of the moving platforms before and after calibration are shown in Fig. 7.

To make the reduction and comparison of the attitude errors before and after calibration more apparent, the scales on the vertical axes of Fig. 7(e) and (f) are made the same as in Fig. 7(a) and (b). As can be seen from the figures, the attitude errors of the moving platforms after calibration are greatly reduced compared with before the calibration. For the attitudes of group 1 of the moving platforms, a phenomenon in which α slightly worsens can be occasionally seen, whereas the attitudes of all other groups significantly improve. The attitude errors of groups 3 and 7 of moving platform 1 appear to disappear altogether, which indicates that the two groups of attitude errors obtain the best calibration effect. In addition, the error value of γ is much larger than that of α and β before calibration, and the error values of the three attitudes are close after calibration. The results show that the calibration method is robust to the initial errors of the manipulator.

To further verify that the kinematic accuracy can be improved through a kinematic calibration, the absolute maximum and absolute mean values of the attitude errors for the two moving platforms before and after calibration are listed in Table V. As observed in the table, the two attitude errors

https://doi.org/10.1017/S0263574718000073 Published online by Cambridge University Press

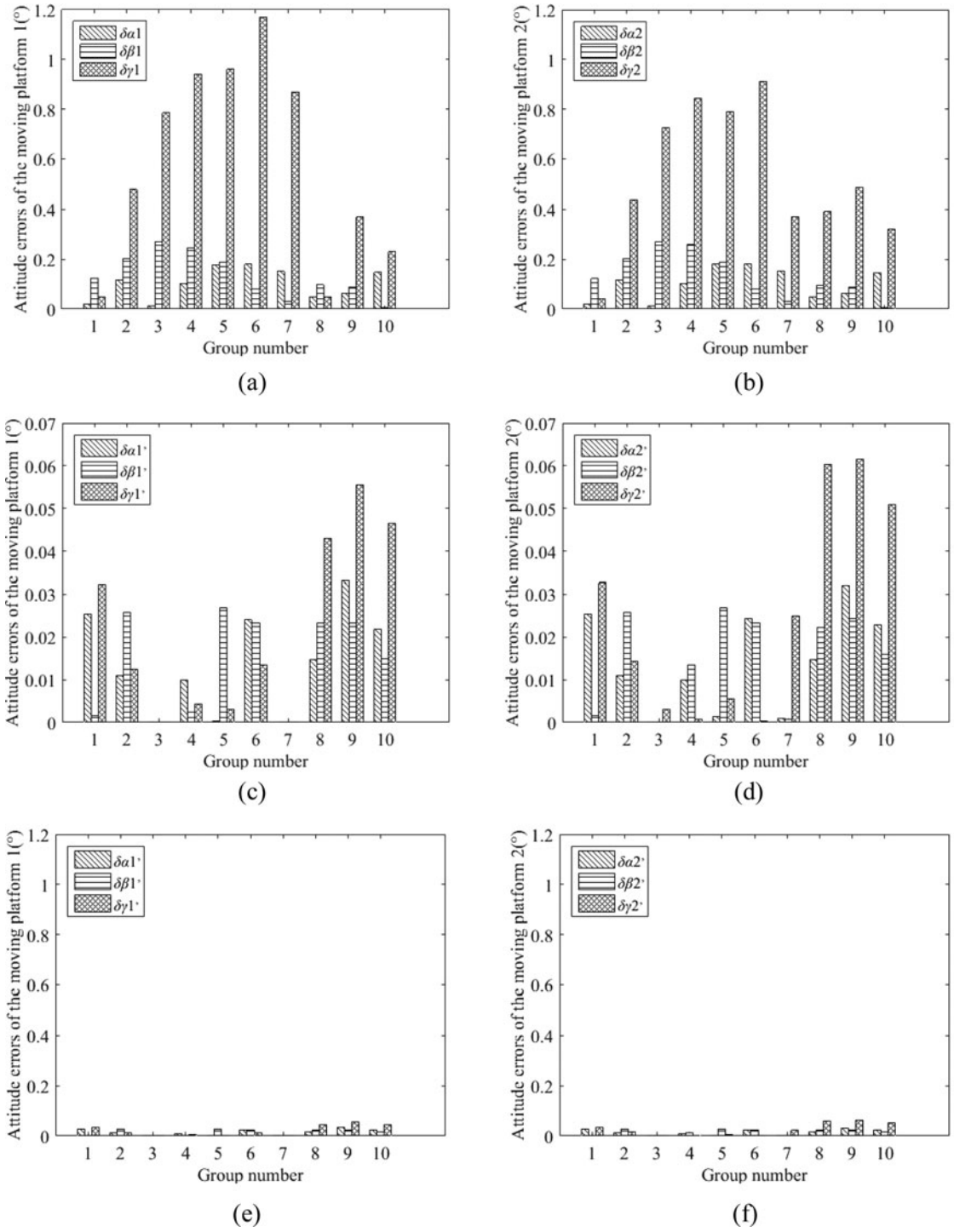

Fig. 7. Attitude errors of moving platforms before and after calibration. (a) Attitude errors of moving platform 1 before calibration ($\delta\alpha1$, $\delta\beta1$, $\delta\gamma1$). (b) Attitude errors of moving platform 2 before calibration ($\delta\alpha2$, $\delta\beta2$, $\delta\gamma2$). (c) Attitude errors of moving platform 1 after calibration ($\delta\alpha1'$, $\delta\beta1'$, $\delta\gamma1'$). (d) Attitude errors of moving platform 2 after calibration ($\delta\alpha2'$, $\delta\beta2'$, $\delta\gamma2'$). (e) Attitude errors of moving platform 1 after calibration ($\delta\alpha1'$, $\delta\beta1'$, $\delta\gamma1'$). (f) Attitude errors of moving platform 2 after calibration ($\delta\alpha2'$, $\delta\beta2'$, $\delta\gamma2'$).

after calibration are significantly less than those before the calibration. For moving platform 1, the absolute maximum value of the attitude errors is reduced from (0.1805, 0.2609, 1.1700)° to (0.0331, 0.0269, 0.0556)°, and the absolute mean value is reduced from (0.1020, 0.1330, 0.5907)° to (0.0141, 0.0142, 0.0210)°. For moving platform 2, the absolute maximum value of the attitude errors is reduced from (0.1804, 0.2690, 0.8430)° to (0.0320, 0.0268, 0.0616)°, and the absolute mean value is reduced

https://doi.org/10.1017/S0263574718000073 Published online by Cambridge University Press

from (0.1022, 0.1341, 0.5322)° to (0.0143, 0.0154, 0.0254)°. It can be seen that, after the kinematic calibration is completed, $\delta\alpha$ and $\delta\beta$ decrease to about 1/10 before calibration, and $\delta\gamma$ decreases to about 1/20. The results indicate that the kinematic accuracy of the manipulator is improved significantly, and the calibration method is therefore effective.

5. Conclusion

The kinematic accuracy of a 2(3HUS+S) parallel manipulator for the simulation of hip joint motions was described in this paper. A D–H coordinate system was established, and a kinematic equation was obtained. A D–H transformation matrix was used as the error-modeling tool and a kinematic error model of the parallel manipulator integrating manufacturing and assembly errors was established based on the perturbation theory. In the modeling, the installation position errors of the moving platforms, errors in the distribution angle of the joints and linear modules and the axis offset and angle errors of the joints were considered, along with errors in the joint lever lengths and position errors of the joints and sliders.

An iterative Levenberg–Marquardt algorithm based on the least squares method was used to identify the geometric errors in the error model according to the error equation and the objective function. To verify the effectiveness of the proposed method, a calibration experiment was carried out. Based on the actual attitudes of the experimentally measured moving platforms, a simulation was realized using MATLAB software, and the identification values of the geometric errors were obtained. Error compensation was completed by regarding the identification values as error compensation values and substituting them into the control software of the manipulator as a means to modify the kinematic model. The experiment and simulation results show that the attitude errors of the moving platforms after calibration are greatly reduced compared with those before calibration, and the kinematic accuracy of the manipulator is significantly improved. The analyses described herein validate the correctness and effectiveness of the error model and kinematic calibration method of the 2(3HUS+S) parallel manipulator.

Acknowledgments

Financial support for this work, provided by the Priority Academic Program Development of Jiangsu Higher Education Institutions and the National Natural Science Foundation of China (Grant No. 91648105), are gratefully acknowledged.

References

1. S. Winiarski, K. Aleksandrowicz, S. Jarzab, A. Pozowski and A. Rutkowska-Kucharska, "Assessment of gait after bilateral hip replacement. Case study," *Ortopedia Traumatologia Rehabilitacja* **16**(2), 197–208 (2014).
2. F. D. Puccio and L. Mattei, "Biotribology of artificial hip joints," *World J. Orthopedics* **6**(1), 77–94 (2015).
3. S. Affatato, A. Spinelli, M. Zavalloni, C. Mazzega-Fabbro and A. Viceconti, "Tribology and total hip joint replacement: Current concepts in mechanical simulation," *Med. Eng. Phys.* **30**(10), 1305–1317 (2008).
4. G. Cheng, Y. Li, L. L. Feng, X. L. Shan and J. H. Yang, "Configuration bifurcation and self-motion analysis of 3SPS+1PS bionic parallel test platform for hip joint simulator," *Mech. Mach. Theory* **86**, 62–72 (2015).
5. Y. J. Zhao, "Singularity, isotropy, and velocity transmission evaluation of a three translational degrees-of-freedom parallel robot," *Robotica* **31**(31), 193–202 (2013).
6. A. Ruiz, F. J. Campa, C. Roldan-Paraponiaris, O. Altuzarra and C. Pinto, "Experimental validation of the kinematic design of 3-PRS compliant parallel mechanisms," *Mechatronics* **39**, 77–88 (2016).
7. R. E. Sanchez-Alonso, J. J. Gonzalez-Barbosa, E. Castillo-Castaneda and J. Gallardo-Alvarado, "Kinematic analysis of a novel 2(3-RUS) parallel manipulator," *Robotica* **34**(10), 2241–2256 (2016).
8. Y. Lu, P. Wang, S. H. Zhao, B. Hu, J. D. Han and C. P. Sui, "Kinematics and statics analysis of a novel 5-DoF parallel manipulator with two composite rotational/linear active legs," *Robot. Comput. Integr. Manuf.* **30**(1), 25–33 (2014).
9. S. Briot and I. A. Bonev, "Accuracy analysis of 3-DOF planar parallel robots," *Mech. Mech. Theory* **43**(4), 445–458 (2008).
10. G. H. Cui, H. Q. Zhang, D. Zhang and F. Xu, "Analysis of the kinematic accuracy reliability of a 3-DOF parallel robot manipulator," *Int. J. Adv. Robot. Syst.* **12, 15** (2015).
11. J. X. Fu, F. Gao, W. X. Chen, Y. Pan and R. F. Lin, "Kinematic accuracy research of a novel six-degree-of-freedom parallel robot with three legs," *Mech. Mach. Theory* **102**, 86–102 (2016).

12. Y. Z. Chen, F. G. Xie, X. J. Liu and Y. H. Zhou, "Error modeling and sensitivity analysis of a parallel robot with SCARA (selective compliance assembly robot arm) motions," *Chin. J. Mech. Eng.* **27**(4), 693–702 (2014).
13. A. Dumlu and K. Erenturk, "Modeling and trajectory tracking control of 6-DOF RSS type parallel manipulator," *Robotica* **32**(4), 643–657 (2014).
14. P. J. Bai, J. P. Mei, T. Huang and D. J. Chetwynd, "Kinematic calibration of Delta robot using distance measurements," *Proc. Inst. Mech. Eng. Part C-J. Mech. Eng. Sci.* **230**(3), 414–424 (2016).
15. H. Chanal, E. Duc, J. Y. Hascoet and P. Ray, "Reduction of a parallel kinematics machine tool inverse kinematic model with regard to machining behavior," *Mech. Mach. Theory* **44**(7), 1371–1385 (2009).
16. A. H. Chebbi, Z. Affi and L. Romdhane, "Prediction of the pose errors produced by joints clearance for a 3-UPU parallel robot," *Mech. Mach. Theory* **44**(9), 1768–1783 (2009).
17. T. Sun, Y. P. Zhai, Y. M. Song and J.T. Zhang, "Kinematic calibration of a 3-DoF rotational parallel manipulator using laser tracker," *Robot. Comput.-Integr. Manuf.* **41**, 78–91 (2016).
18. C. Fan, G. L. Zhao, J. Zhao, L. Zhang and L. N. Sun, "Calibration of a parallel mechanism in a serial-parallel polishing machine tool based on genetic algorithm," *Int. J. Adv. Manuf. Technol.* **81**(1–4), 27–37 (2015).
19. W. J. Tian, F. W. Yin, H. T. Liu, J. H. Li, Q. Li, T. Huang and D. G. Chetwynd, "Kinematic calibration of a 3-DOF spindle head using a double ball bar," *Mech. Mach. Theory* **102**, 167–178 (2016).
20. L. P. Wang, F. G. Xie, X. J. Liu and J. S. Wang, "Kinematic calibration of the 3-dof parallel module of a 5-axis hybrid milling machine," *Robotica* **29**(4), 535–546 (2011).
21. Y. J. Chiu and M. H. Perng, "Self-calibration of a general hexapod manipulator with enhanced precision in 5-DOF motions," *Mech. Mach. Theory* **39**(1), 1–23 (2004).
22. X. D. Ren, Z. R. Feng and C. P. Su, "A new calibration method for parallel kinematics machine tools using orientation constraint," *Int. J. Mach. Tools Manuf.* **49**(9), 708–721 (2009).
23. Y. Bai, H. Q. Zhuang and D. L. Wang, "Apply fuzzy interpolation method to calibrate parallel machine tools," *Int. J. Adv. Manuf. Technol.* **60**(5–8), 553–560 (2012).
24. D. Zhang and Z. Gao, "Optimal kinematic calibration of parallel manipulators with pseudoerror theory and cooperative coevolutionary network," *IEEE Trans. Ind. Electron.* **59**(8), 3221–3231 (2012).
25. X. L. Shan, G. Cheng and X. Z. Liu, "Note: Application of a novel 2(3HUS+S) parallel manipulator for simulation of hip joint motion," *Rev. Sci. Instrum.* **87**(7), 149–151 (2016).

https://doi.org/10.1017/S0263574718000073 Published online by Cambridge University Press